CHAPTER W13

Ceramics

W13.1 Ternary Phase Diagrams

As the number of components of a system increases, the number of possible subsystems increases rapidly and the complexity grows exponentially. For example, a two-component system has only two possible unary subsystems and one binary subsystem for a total of three different types of subsystems. A three-component system has three unary subsystems, three binary subsystems, and a ternary subsystem, for a total of seven different types of subsystems. In the general case a C-component system will have $C!/[C'!(C - C')!]$ subsystems with C' components, and will have a total of $2^C - 1$ possible subsystems. Often, it is desirable to optimize a particular physical property of the system, so the composition and temperature must be chosen carefully to achieve this optimization. Obviously, the process becomes more challenging as the number of components is increased. Phase diagrams provide a type of road map upon which it is possible to chart the composition of the material and indicate the various phase boundaries.

Often, materials with interesting physical properties are constructed out of just three components, which will be labeled by A, B, and C. These may be elements or compounds. For example, the electro ceramic $Pb_xZr_yTi_zO_3$ (PZT) is constructed from the compounds $A = PbO$, $B = TiO_2$, and $C = ZrO_2$, and the composition is $(PbO)_x \cdot (ZrO_2)_y \cdot (TiO_2)_z$. Here x, y, and z are constrained by the valence balance condition $2x + 4y + 4z = 6$, so that only two of the variables may be varied independently. The high-temperature superconductor $YBa_2Cu_3O_{7-x}$ is but one of many phases constructed from Y_2O_3, BaO, and Cu_2O. Glasses are often made from ternary mixtures, such as soda-lime, made from SiO_2, CaO, and Na_2O.

According to the Gibbs phase rule (see Section W6.4), Eq. (W6.9), the number of degrees of freedom, F, is related to the number of components, C, and the number of phases, P, by $F = C - P + 2$. For constant temperature and pressure, two of the degrees of freedom are removed, leaving $F' = C - P$ degrees of freedom. For a three-component system, such as PZT, $C = 3$. Since there must be at least one phase present, $p \geq 1$ and $F' \leq 2$. The two degrees of freedom are conveniently displayed using the Gibbs triangle, as illustrated in Fig. W13.1.

Imagine that there is a totality of one unit of components, so the chemical formula is $A_aB_bC_c$, with $a + b + c = 1$ and (a, b, c), each lying in the range 0 to 1. The composition may be represented graphically as a point inside an equilateral triangle. The height of this triangle is taken to be 1. In Fig. W13.1 point O represents $A_aB_bC_c$. The perpendicular distances to the sides of the triangle are a, b, and c, and the fractions of components A, B, and C present are also a, b, and c. The corners of the triangle represent pure-component (unary) compounds. If the point O were at A, then

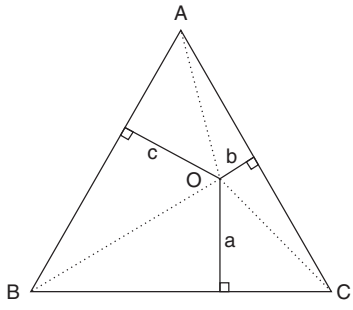

Figure W13.1. Point O represents the composition $A_aB_bC_c$, where $a + b + c = 1$.

$b = c = 0$ and $a = 1$. The composition would be 100% A. The edges of the triangle represent binary compounds. For example, a point on the base of the triangle will have composition B_bC_c, with $b + c = 1$. If the point O is at the center of the triangle, then $a = b = c = \frac{1}{3}$ and 33.3% of each component is present.

It is a simple matter to prove that $a + b + c = 1$. Note that the area of equilateral triangle ABC (with side $L = 2/\sqrt{3}$) is half the base times the height: $(\frac{1}{2})(L)(1) = 1/\sqrt{3}$. On the other hand, the area of ABC may be written as the sums of the areas of the three triangles AOB, BOC, and COA, which gives $1/\sqrt{3} = (\frac{1}{2})L(a + b + c)$, so $a + b + c = 1$. Thus any point within the triangle ABC will always correspond to a total of one unit of components.

An alternative method for determining the composition is to make the construction shown in Fig. W13.2. Lines are passed through point O parallel to the three sides. The intersections of these lines with the sides are labeled by the points D, E, F, G, H, and I. It can be shown that the relative amounts of A, B, and C present are proportional to the lengths of segments of the sides, that is,

$$\frac{c}{\text{AI}} = \frac{b}{\text{IH}} = \frac{a}{\text{HC}}, \quad \frac{a}{\text{FG}} = \frac{b}{\text{GC}} = \frac{c}{\text{BF}}, \quad \frac{c}{\text{DE}} = \frac{a}{\text{EB}} = \frac{b}{\text{AD}}. \tag{W13.1}$$

This construction may be generalized to the case of a scalene triangle. In Fig. W13.3, point O represents 1 mol of material with composition $A_aB_bC_c$, where $a + b + c = 1$. Through point O, construct-lines FOI, HOE, and DOG are drawn parallel to sides CB, AC, and BA, respectively. Each side is divided into three segments by these lines. It may be shown that the following identity holds for the lengths of the segments:

$$\text{DE:EC:BD} = \text{CF:FG:GA} = \text{IB:AH:HI} = a\text{: } b\text{: } c. \tag{W13.2}$$

The ternary diagram is used to depict the various phases of the material at thermal equilibrium. At times one is interested only in the phase boundaries at a given temperature and pressure. The diagram is then called an *isothermal-ternary diagram*. Alternatively, the temperature field could be represented by drawing isothermal contours on the diagram. Since this proves to be more useful, this representation will be used here.

Refer to Fig. W13.4, where a three-dimensional temperature–composition diagram is drawn. Viewed from the top, one has a ternary phase diagram. This diagram will be used to follow a process in which a liquid solidifies. At sufficiently high temperatures

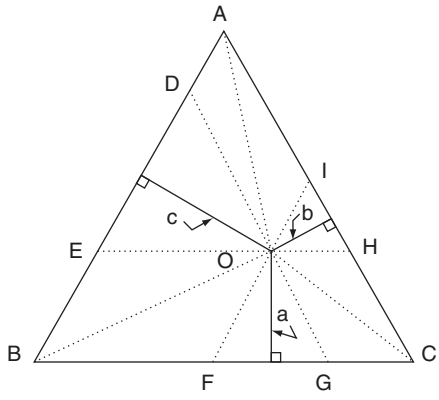

Figure W13.2. Material $A_aB_bC_c$ is represented by point O. The segments AI:IH:HC are in the same proportion as $c:b:a$.

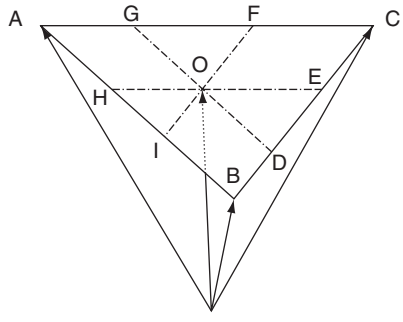

Figure W13.3. Composition triangle ABC together with various construction lines.

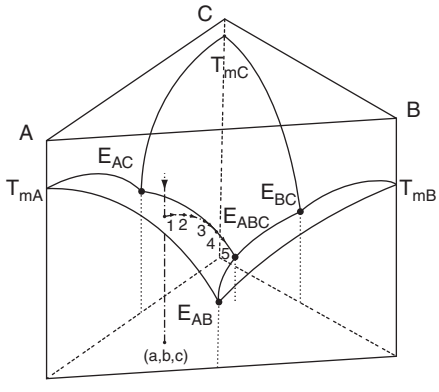

Figure W13.4. Three sheets of the liquidus surface on a plot of temperature versus composition.

the material is assumed to be liquid. As the temperature is slowly lowered, the material begins to crystallize. The degree of crystallization, and the fractions and compositions of solid and liquid formed, are determined by the liquidus surfaces. Of course, the mean composition taken over all the phases always remains the same. In Fig. W13.4 the liquidus surface is presented for the simple case in which solid solutions are not formed. The liquidus surface consists of three separate sheets, corresponding to the three primary compositions A, B, and C. Various eutectic points are depicted by the letter E with subscripts. Thus E_{AB} denotes the eutectic point for the composition A_aB_b for the special case where $a + b = 1$ and $c = 0$. E_{ABC} is the ternary eutectic point and is the lowest point for which some liquid remain. There is a horizontal eutectic plane (not shown) in the phase diagram passing through the point E_{ABC} below which only completely solid material exists. The melting points for the pure components are denoted by $T_{m\mathrm{A}}$, $T_{m\mathrm{B}}$, and $T_{m\mathrm{C}}$.

Shown on Fig. W13.4 is a cooling path for a liquid with composition (a, b, c). As the temperature is lowered, point 1 is encountered and solid phase A begins to nucleate. Further reduction of the temperature causes an increased growth of phase A and a modification of the composition of the liquid. The liquid composition is determined by the curve 1–2–3–4–5. Along 1–2–3, only solid phase A and a liquid are present. At point 3, phase C begins to nucleate. Along path 3–4–5 (which is the valley between sheets A and C), phases A and C and a liquid of varying composition are present. At point 5 the liquid reaches the ternary eutectic composition. At a lower temperature, only solid phases A, B, and C exist, with the original composition (a, b, c).

Figure W13.5 depicts the same scenario as in Fig. W13.4 but viewed from above. The isothermal contours are not shown but are there implicitly. Note that A–1–2–3 is a straight line. Along line 1–2–3 the composition may be determined by applying the lever rule. Thus at a temperature corresponding to T_1, the liquid will have composition (a_1, b_1, c_1). The amounts of liquid and phase α at $T = T_2$ are in the ratio of the distances d_{A1}/d_{12}. At temperature T_3 the liquid has composition (a_3, b_3, c_3) and the liquid to phase α ratio is d_{A1}/d_{13}. At points 4 and 5 the compositions are such that the center of gravity of points A, C, 4, or 5 lies at the original point 1.

There are numerous other possibilities for drawing the phase diagrams but they will not be covered exhaustively here. The principles of analysis are similar. Several points are worth mentioning, however. Stoichiometric binary compounds (e.g., A_mB_n,

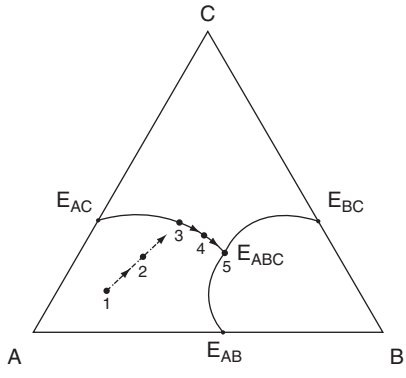

Figure W13.5. Path toward solidification on the ternary phase diagram.

with m and n integers) are represented by points on the appropriate edge (AB in this case). Stoichiometric ternary compounds (e.g., $A_mB_nC_j$, with m, n, and j integers) appear as points in the interior of the triangle. These points are usually surrounded by a domain of influence bounded by a phase boundary. An example of this will be encountered in Section 13.7 of the textbook[†] when the ternary phase diagram for the glass-forming region of $Na_2O \cdot CaO \cdot SiO_2$ is discussed (see Fig. 13.15). The net result is that the ternary phase diagram often has the appearance of a mosaic with numerous phases indicated. Often, there is a definite crystalline order associated with a stoichiometric phase. Points with nearby compositions may be thought of as crystals possessing defects. The farther one goes from the stoichiometric point, the larger the number of defects. When a sufficient number of defects occur, a phase transition to another crystal structure may result.

As mentioned earlier, it is possible to have as many as three distinct phases present at once (i.e., $P = 3$). In that case, the effective number of degrees of freedom for a ternary system is $F = C - P = 0$. Consider the Gibbs triangle depicted in Fig. W13.6, which shows three phases (α, β, γ) to be present. Since $F = 0$, the composition of the material at point O is uniquely determined: the fractions of the various phases present are (f_α, f_β, f_γ), where $f_\alpha + f_\beta + f_\gamma = 1$. For the point O, the composition (a, b, c) will be determined by solving the matrix equation

$$\begin{bmatrix} a \\ b \\ c \end{bmatrix} = \begin{bmatrix} a_\alpha & a_\beta & a_\gamma \\ b_\alpha & b_\beta & b_\gamma \\ c_\alpha & c_\beta & c_\gamma \end{bmatrix} \begin{bmatrix} f_\alpha \\ f_\beta \\ f_\gamma \end{bmatrix}. \tag{W13.3}$$

In Fig. W13.7 a sequence of four isothermal sections is illustrated, corresponding to the temperatures $T_1 > T_2 > T_3 > T_4$ for an idealized ternary system. Temperature T_1 is above the liquidus surface, so any point in the phase diagram corresponds to a homogeneous liquid. At temperature T_2 it is assumed that part of the liquidus surface is above the isothermal plane and part below. It is assumed that there are compositional ranges for which the phases α, β, and γ coexist with the liquid phase, as illustrated in

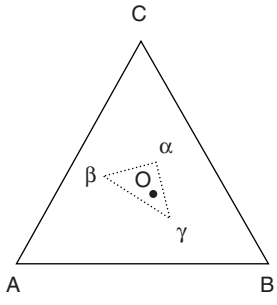

Figure W13.6. Gibbs triangle with a three-phase field. There is a unique admixture of the three phases at point O.

[†] The material on this home page is supplemental to *The Physics and Chemistry of Materials* by Joel I. Gersten and Fredrick W. Smith. Cross-references to material herein are prefixed by a "W"; cross-references to material in the textbook appear without the "W."

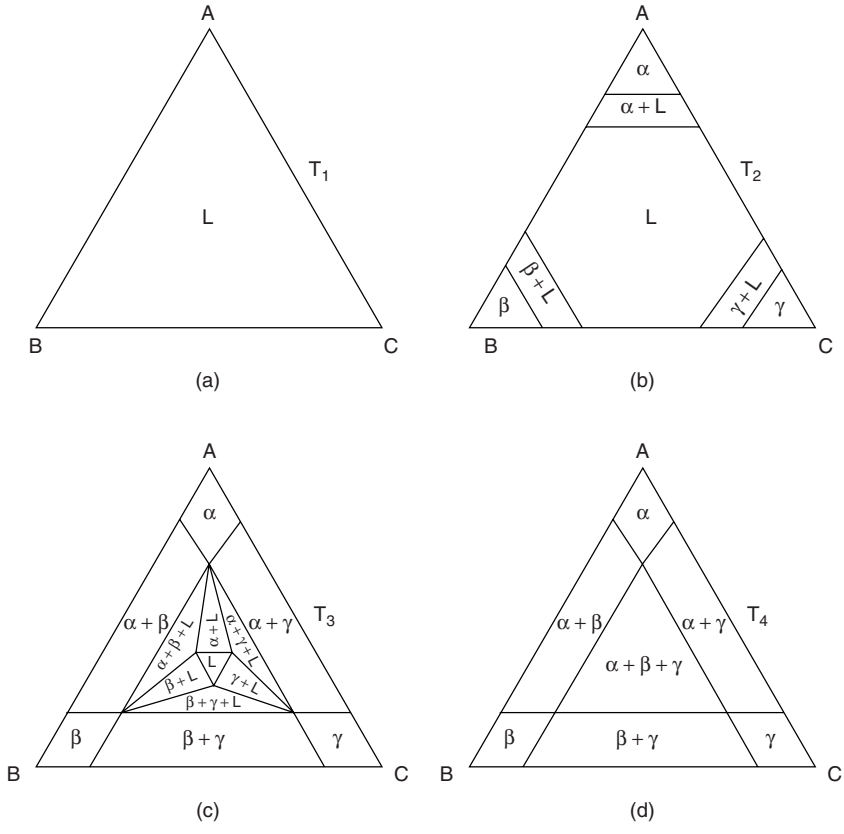

Figure W13.7. Sequence of four isothermal phase diagrams, illustrating the presence of various phases.

the figure. At T_3 the temperature is slightly above the three-phase eutectic temperature. One now finds the coexisting binary solid phases $\alpha + \beta$, $\beta + \gamma$, and $\alpha + \gamma$. There are also regions corresponding to the coexistence of the unary phases with the liquid, $\alpha + L$, $\beta + L$, and $\gamma + L$, as well as regions consisting of the coexistence of the two phases with the liquid, $\alpha + \beta + L$, $\beta + \gamma + L$, and $\alpha + \gamma + L$. At T_4, below the eutectic temperature, only solid phases are present: the unary phases α, β, or γ; the two-phase regions $\alpha + \beta$, $\beta + \gamma$, or $\alpha + \gamma$; and the three-phase region $\alpha + \beta + \gamma$.

It is important to stress that the phase diagram applies only for thermal equilibrium. Nevertheless, for rapid cooling, the diagram may be used as an intuitive guide to understanding solidification. The composition of the microstructure that will form may be estimated in much the same way as in the study of metals (see Section 6.5 and Figs. 6.9 and 6.10). The faster the material passes through a given phase domain as the sample is cooled, the less time there is available for nucleation and growth of that equilibrium phase to occur.

W13.2 Silicates

Silicon and oxygen are the two most abundant elements in Earth's crust. There is a broad class of minerals based on combinations of Si and O and other elements called

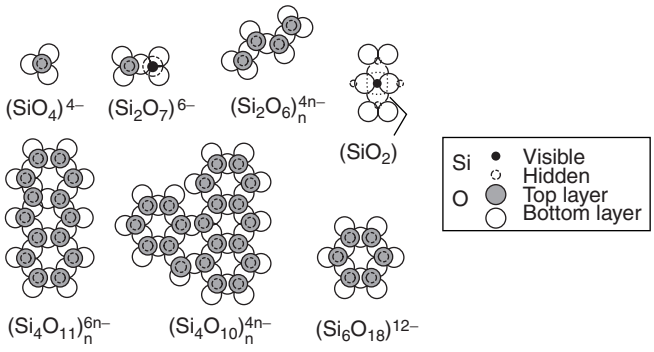

Figure W13.8. Schematic representation of the seven classes of silicate ions. There are O^{2-} ions residing at the corners of the tetrahedra and Si^{4+} ions at their centers. (Adapted from H. W. Jaffe, *Crystal Chemistry and Refractivity*, Dover, Mineola, N.Y., 1996.)

silicates. An appreciation of the various ions formed from Si and O permit one to understand more complex structures in which other cations, such as Al, substitute for the Si ions.

The valence of Si is +4 and that of O is −2. A basic ion formed is the $(SiO_4)^{4-}$ ion. The Si^{4+} resides at the center of a tetrahedron, and the O^{2-} ions are at the vertices. The bond is about equally covalent and ionic and is very strong. The tetrahedra may be connected in a variety of ways to form complex ions. Figure W13.8 depicts the basic structures. There are seven principal classes of silicates. Orthosilicates (also known as nesosilicates or island silicates), such as forsterite (Mg_2SiO_4), olivine ($Mg_xFe_{2-x}SiO_4$), and zircon ($ZrSiO_4$), are based on independent $(SiO_4)^{4-}$ tetrahedra linked by divalent cations. In place of the $(SiO_4)^{4-}$ ion, there could be substituted the $(AlO_4)^{5-}$ ion. An example of this is the synthetic crystal YAG [yttrium aluminum garnet, $Y_3Al_2(AlO_4)_3$], used as a laser crystal. In the sorosilicates there are two tetrahedra joined vertex to vertex, sharing a common oxygen to form the $(Si_2O_7)^{6-}$ ion. An example is the mineral thortveitite [$Sc_2(Si_2O_7)$]. The structure with a triad of tetrahedra corner-sharing one oxygen ion to form the $(Si_3O_9)^{6-}$ ion does not seem to be found in nature. In the cyclosilicates, such as the gemstone beryl ($Be_3Al_2Si_6O_{18}$), the tetrahedra are arranged in hexagonal rings corner-sharing six oxygens to create $(Si_6O_{18})^{12-}$ ions. In the inosilicates, such as the mineral jadeite [$NaAl(Si_2O_6)$], tetrahedra form a linear chain with corner-shared oxygens to produce an ion of the form $(SiO_3)_n^{2n-}$. In the phyllosilicates, such as mica or talc [$Mg_3(Si_2O_5)_2(OH)_2$], the basic ionic unit is the $(Si_2O_5)^{2-}$ ion. In the amphiboles (or double-chain silicates) two parallel inosilicate chains link together so that every second tetrahedron has a corner-shared oxygen, producing the ion $(Si_4O_{11})_n^{6n-}$. An example is the mineral tremolite [$Ca_2Mg_5(Si_4O_{11})_2(OH)_2$]. The final class of silicate is the tektosilicate, based on the neutral SiO_2 subunit. An example of this is quartz itself, with the composition SiO_2, or anorthite [$CaOAl_2O_3(SiO_2)_2$]. The results are summarized in Table W13.1.

An oxygen shared by two tetrahedra is called a *bridging oxygen*. One that is not shared is called a *nonbridging oxygen* (NBO). One may classify the structures according to the number of nonbridging oxygens that the tetrahedra possess, as shown in Table W13.1. Tektosilicates have no NBOs, or equivalently, four shared corners. The structural unit is neutral and is based on SiO_2. Disilicates have only one NBO

TABLE W13.1 Seven Principal Classes of Silicates

Class	Ion	Shared Corners	Nonbridging Oxygens
Nesosilicate	$(SiO_4)^{4-}$	0	4
Sorosilicate	$(Si_2O_7)^{6-}$	1	3
Cyclosilicate	$(Si_6O_{18})^{12-}$	2	2
Inosilicate	$(SiO_3)_n^{2n-}$	2	2
Amphibole	$(Si_4O_{11})_n^{6n-}$	2, 3	2, 1
Phyllosilicate	$(Si_2O_5)^{2-}$	3	1
Tektosilicate	(SiO_2)	4	0

Source: Data from H. W. Jaffe, *Crystal Chemistry and Refractivity*, Dover, Mineola, N.Y., 1996.

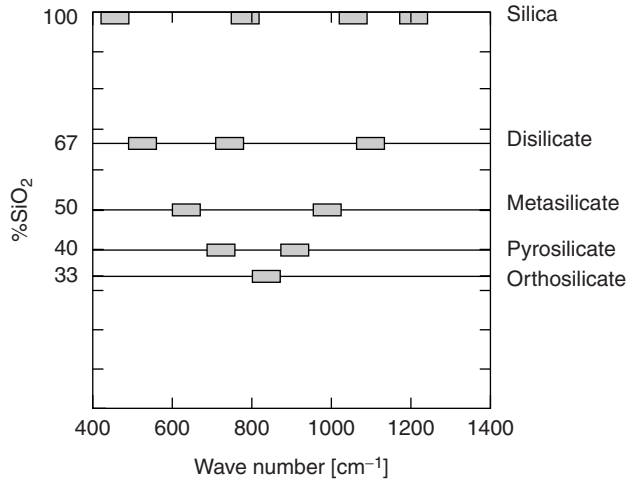

Figure W13.9. Ranges of Raman shifts for various silicates. [Adapted from P. F. McMillan, *Am. Mineral.*, **69**, 622 (1984).]

or, equivalently, three shared corners, and the ion is $(Si_2O_5)^{2-}$. Metasilicates have two NBOs (i.e., two shared corners) and the ion is $(SiO_3)^{2-}$. Pyrosilicates have three NBOs (i.e., one shared corner) and the ion is $(Si_2O_7)^{6-}$. Orthosilicates have four NBOs, hence no shared corners, and are based on the $(SiO_4)^{4-}$ ion.

Raman scattering may be used to identify the various ions. In Fig. W13.9 the ranges of the Raman bands for the various ions in silicate glasses are depicted by the shaded areas. In silicates there are cations present in addition to the silicate ions, so that one may regard the materials as part silica and part foreign cations. The ordinate of Fig. W13.9 gives the percentage of the material that is SiO_2. Silica, of course, is 100% SiO_2. The 400-cm^{-1} peak is associated with a rocking motion in which the Si–O–Si angle remains fixed but the oxygen rocks back and forth perpendicular to the initial Si–O–Si plane. The 800-cm^{-1} peak corresponds to a bending motion of the Si–O–Si bond angle. The peak at 1100 to 1200 cm^{-1} is due to a stretching motion of the Si–O bond. In the orthosilicates, the bending motion of the Si–O–Si bond is responsible for the 800-cm^{-1} peak. In the pyrosilicates two tetrahedra are joined together. The bending motions could be either in phase or out of phase. As a result, the 800-cm^{-1}

peak is split into two peaks, one at a higher frequency and the other at a lower one. A normal-mode analysis of the silicate ions leads to a more detailed description of the correlation of peak location with ion type.

W13.3 Clay

Shards of pottery excavated in scattered archeological sites around the world testify to the role that clay has played since antiquity as a primary technological material. Clays are layered aluminosilicates, being composed primarily of Al, Si, O, and H with varying degrees of alkali, alkaline earths, or Fe. Some common clays found in nature include kaolinite, pyrophyllite, and talc. They are members of a mineral family called phyllosilicates that include micas, such as muscovite, as well as serpentines and chlorites. Clays are crystalline materials that have a small particle size. When combined with water they become hydroplastic (i.e., they are readily moldable). When heated, the particles fuse together while the overall macroscopic shape is retained. Upon cooling, the molded shape becomes the desired object.

There are two types of primary layers in the clay structure. One is a 0.22-nm layer composed of SiO_4 tetrahedra joined by their corners in a hexagonal array (Fig. W13.10*a*). The bases are coplanar and the tips of the tetrahedra all point in the same direction. At the vertices are either O atoms or OH radicals. The second primary layer is a 0.22-nm sheet of octahedra containing Al at the center which are sixfold coordinated with O atoms or OH radicals at the vertices (Fig. W13.10*b*). [In the case where there are only hydroxyl radicals, it is the mineral gibbsite, $Al_2(OH)_6$]. The various types of clay differ from each other in the number of these sheets, the

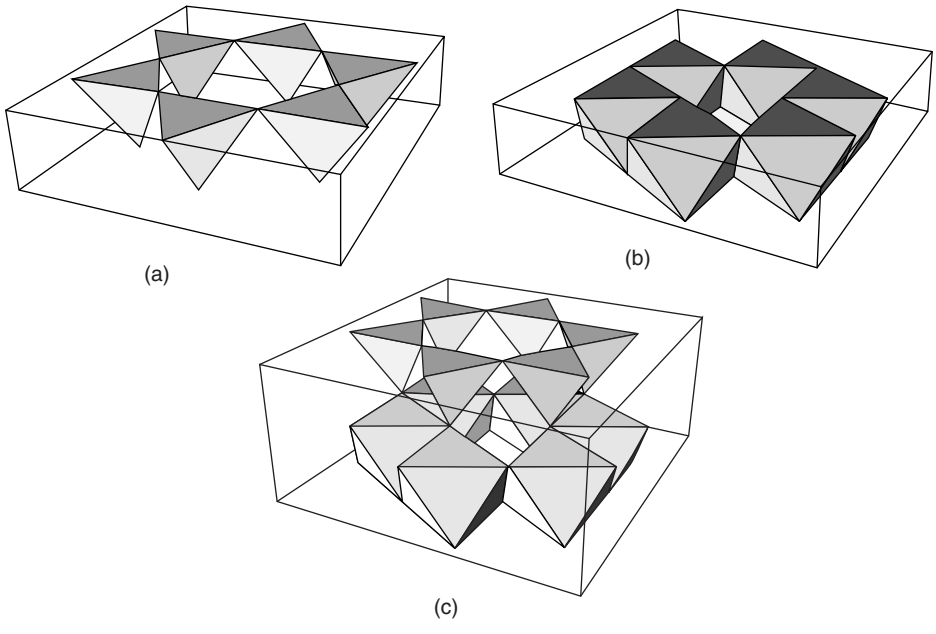

Figure W13.10. (*a*) Silica layer; (*b*) gibbsite layer; (*c*) kaolinite layer.

replacement of some Al or Si by other elements, or by the presence of sheets of water between the layers.

Kaolinite [$Al_2Si_2O_5(OH)_4$] has a 1:1 structure (i.e., the bilayer consists of one silica layer and one gibbsite layer). The overall thickness is 0.716 nm (0.22 nm for the tetrahedra + 0.22 nm for the octahedra + 0.276-nm spacing). The silica tetrahedra (SiO_4) point toward the gibbsite sheet, with the oxygens on the basal plane of the silica forming one outer surface and the hydroxyls of the gibbsite forming the second outer surface. The Al ions lie on a hexagonal lattice with two-thirds of the possible sites filled. Successive bilayers have the same orientation and are bound to each other by hydrogen bonding. A schematic of this arrangement (with the two sheets separated from each other for illustration purposes) is drawn in Fig. W13.10*c*. The atomic positions in the successive layers are sketched in Fig. W13.11. Figure W13.11*a* shows the basal O^{2-} plane with Si^{4+} atop the midpoint of the triangles formed by the oxygens; Fig. W13.11*b* shows O^{2-} ions above the Si^{4+} ions, completing the *tetrahedral layer* (T layer); Fig. W13.11*c* shows the positions of the Al^{3+} ions and OH^- ions in the same layer as the aforementioned O^{2-} ions. The OH^- layers lie above the voids in the basal layer. Finally, Fig. W13.11*d* shows a top layer with OH^- ions. Each Al^{3+} ion is surrounded by six negative ions. Below each Al^{3+} is a triangle with two O^{2-} ions and one OH^- ion. Above each Al^{3+} is a triangle of three OH^- ions. The orientation of the upper triangle is opposite to that of the lower triangle. The net result is that each Al^{3+} ion sits at the center of an octahedron. The layer is referred to as the *O* layer. The protons of the top OH^- layer are directed away from preceding *O* layer, ready to hydrogen-bond with the next T layer. Thus the stacking sequence in kaolinite may be denoted by TO–TO–TO–$\cdots$. The actual crystal structure is not orthorhombic, as in the sketch, but is slightly triclinic, with parallelipiped unit cell dimensions $(a, b, c) = (0.51, 0.89, 0.72)$ nm and angles $(\alpha, \beta, \gamma) = (91.8^\circ, 104.5^\circ, 90^\circ)$.

The lattice spacings in isolated gibbsite do not precisely match the lattice spacings in silica. When the two layers are brought into registry, one layer is compressed and the

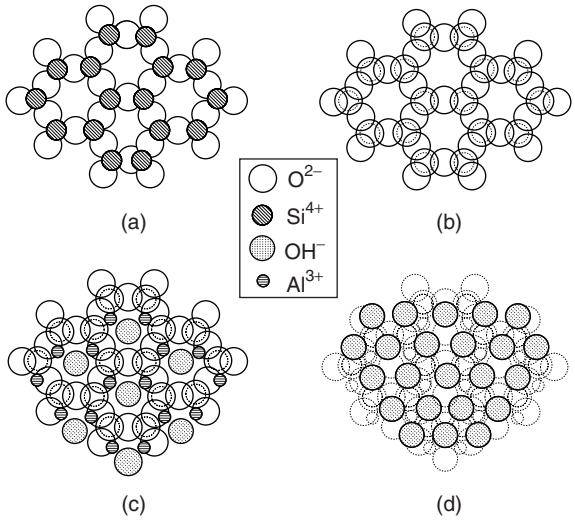

Figure W13.11. Layer-by-layer assembly of a kaolinite sheet. (Adapted from H. W. Jaffe, *Crystal Chemistry and Refractivity*, Dover, Mineola, N.Y., 1996.)

other is stretched. The resulting strain energy grows as the area of the layer increases. Eventually, the layers crack to relieve the strain energy. This limits the extent of the clay particles to a small size.

Pyrophyllite $[Al_2(Si_2O_5)_2(OH)_2]$ differs from kaolinite in that it contains two silica sheets instead of one (i.e., it has a 2:1 composition). The tetrahedra in the silica layers point inward toward the gibbsite core layer, so the outer surface of the trilayer structure consists of oxygen planes. Additional trilayers bond to this by weak van der Waals bonds. The unit cell is monoclinic with dimensions $(a, b, c) = (0.52, 0.89, 1.86)$ nm and angles $\alpha = \beta = 90^\circ$ and $\gamma = 99.9^\circ$.

Talc $[Mg_3(Si_2O_5)_2(OH)_2]$ has the same 2:1 structure as pyrophyllite, with the exception that the two Al^{3+} ions are replaced by three Mg^{2+} ions to maintain the valence requirements. Thus all the sites of the hexagonal lattice are now filled with Mg atoms, as opposed to the two-thirds occupancy for Al. Talc may be thought of as being based on the mineral brucite $[Mg_3(OH)_6]$ rather than on gibbsite, as before. It forms a monoclinic crystal with unit cell dimensions (0.53, 0.91, 1.89) nm and $\beta = 100^\circ$. Closely related is the clay montmorillonite, in which only some of the Al^{3+} are replaced by Mg^{2+} ions. Because of the valence mismatch, additional ions, such as Na^+, must also be incorporated, giving the composition $Al_{2-x}Mg_xNa_x(Si_2O_5)_2(OH)_2$. In the clay illite, some of the Si^{4+} ions are replaced by Al^{3+} ions. The valence mismatch is now compensated by adding K^+ ions to the hexagonal voids of the O layers. The structure is thus $Al_2(Si_{2-x}Al_xK_xO_5)_2(OH)_2$. In the special case where $x = 0.5$, the mica muscovite $[KAl_3Si_3O_{10}(OH)_2]$ is obtained. The K^+ ion serves to ionically bind adjacent trilayers tightly, thereby giving considerable rigidity to the structure.

W13.4 Cement

If limestone (calcite) is heated to 900°C, the reaction $CaCO_3 \rightarrow CaO + CO_2$ occurs and CaO (*quick lime*) is produced. When placed in contact with water, the CaO becomes hydrated and the product is called *slaked lime*. Heat is released, and the material swells and eventually hardens (sets). Mortar is a mixture of quick lime and sand (silica), which, when hydrated, forms a composite material that is used to bind bricks together.

Concrete, a composite material, is the primary structural material in use today. It consists of pebbles and sand bound together by cement.

In this section the focus will be on the most common type of cement, called *Portland cement*. The composition is 60 to 66% CaO (lime), 19 to 25% SiO_2 (silica), 3 to 8% Al_2O_3 (alumina), 1 to 5% Fe_2O_3 (ferrite), up to 5% MgO (magnesia) and 1 to 3% SO_3. When heated, four primary compounds are formed: dicalcium silicate (DCS) ($2CaO{\cdot}SiO_2$), tricalcium silicate (TCS) ($3CaO{\cdot}SiO_2$), tetracalcium aluminoferrite (TCAF) ($4CaO{\cdot}Al_2O_3{\cdot}Fe_2O_3$), and tricalcium aluminate (TCA) ($3CaO{\cdot}Al_2O_3$). Portland cement is, on average (by wt %), 46% TCS, 28% DCS, 8% TCAF, and 11% TCA. In addition, there is 3% gypsum ($CaSO_4{\cdot}2H_2O$), 3% magnesia, 0.5% K_2O or Na_2O, and 0.5% CaO. When water is added, a hydration reaction occurs and heat is generated. The hydrated particles conglomerate and a gel is formed. The cement sets in the course of time.

The four compounds provide various attributes to the cement. Thus DCS hardens slowly and improves the cement's strength after a considerable time (a week). TCS hardens more rapidly, gives the initial set, and provides early strength. TCA also provides early strength and dissipates early heat. TCAF reduces the "clinkering"

temperature where the particles bind together. The chemistry of hydration involves the production of hydrous calcium silicates and aluminates via the following reactions:

$$2(\text{DCS}) + 4H_2O \longrightarrow 3CaO{\cdot}2SiO_2{\cdot}3H_2O + Ca(OH)_2$$

$$2(\text{TCS}) + 6H_2O \longrightarrow 3CaO{\cdot}2SiO_2{\cdot}3H_2O + 3Ca(OH)_2$$

$$\text{TCAF} + 10H_2O + 2Ca(OH)_2 \longrightarrow 6CaO{\cdot}Al_2O_3{\cdot}Fe_2O_3{\cdot}12H_2O$$

$$\text{TCA} + 12H_2O + Ca(OH)_2 \longrightarrow 3CaO{\cdot}Al_2O_3{\cdot}Ca(OH)_2{\cdot}12H_2O$$

$$\text{TCA} + 26H_2O + 3(CaSO_4{\cdot}2H_2O) \longrightarrow 6CaO{\cdot}Al_2O_3{\cdot}3SO_3{\cdot}32H_2O$$

$$6CaO{\cdot}Al_2O_3{\cdot}3SO_3{\cdot}32H_2O + 2(\text{TCA}) + 4H_2O \longrightarrow 3(4CaO{\cdot}Al_2O_3{\cdot}3SO_3{\cdot}12H_2O)$$

The reagent particles, consisting of the hydrated species, typically have sizes in the range 1 to 50 μm and are bound together (flocculated) by polar bonds. The processes above proceed by ionic reactions in water. Calcium hydroxide [$Ca(OH)_2$] nucleates and grows as crystallites ranging in size from 10 to 500 μm, whereas the hydrated calcium silicate or aluminate forms a porous network of bonded colloidal particles. The porosity is determined by the water-to-cement ratio (w/c). If the porosity exceeds 18%, a connected network of pores percolate and permeates the sample. If it reaches 30%, more than 80% of the pores are interconnected. The behavior is typical of a percolating network. For high w/c ratios, it takes more hydration to close off the pore space. If w/c is sufficiently high ($> 60\%$) the pore space is never closed off by hydration.

The flow (rheology) of cement before hardening is described approximately by the viscoelastic equation

$$\sigma = \sigma_B + \eta_{\text{pl}} \frac{d\varepsilon}{dt}, \tag{W13.4}$$

where σ is the applied stress, ε the strain, η_{pl} the plastic viscosity, and σ_B called the Bingham yield stress. The last two parameters depend sensitively on the microstructure of the cement and increase as finer particles are used. Typical values for η_{pl} are between 0.01 and 1 Pa · s, and for σ_B range between 5 and 50 Pa. To get the cement to flow, the hydrogen bonds must be broken, and this accounts for the term σ_B. Viscoelasticity is also seen to be important in the discussion of polymers in Chapter 14.

The strength of cements and concrete is largely a function of how much contact area there is between the respective particles. This is illustrated in Fig. W13.12, where three packing geometries are compared. Figure W13.12*a* symbolizes a close-packed monodisperse (homogeneous in size) set of spherical grains. Figure W13.12*b* shows that by densifying with smaller particles, a higher contact area may be achieved, thereby strengthening the network. Figure W13.12*c* shows that an improper assortment of sizes can weaken the network.

One of the main limitations of cement is its brittleness. Crack propagation is partially limited by the pores and other flaws in the material. It has been found that by embedding small fibers, crack propagation can be largely arrested and the cement may be toughened considerably.

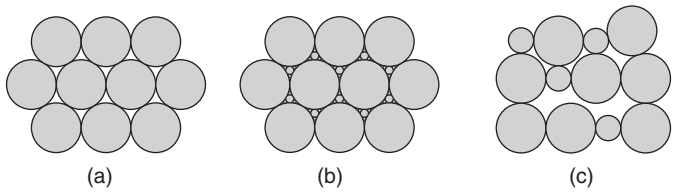

Figure W13.12. Comparison of three packing geometries for spherical particles.

Appendix W13A: Radius Ratios and Polyhedral Coordination

The relationship between the radius ratio and the polyhedral coordination may be derived by examining typical bonding configurations. In Fig. W13A.1 a planar arrangement of four ions is shown. The smaller ion is the cation, with radius r_c, and the larger ion is the anion, with radius r_a. In all cases the cation-to-anion distance will be given by $a = r_c + r_a$, since the cation and anion are in contact. The anion-to-anion distance will be denoted by d. Note that for all cases to be considered, $d \geq 2r_a$, since it is assumed that the anions cannot overlap. From Fig. W13A.1, since the angle between any two a-vectors is 120°, it follows that $d = a\sqrt{3}$. The condition for triangular bonding thus becomes

$$(r_c + r_a)\sqrt{3} \geq 2r_a, \tag{W13A.1}$$

which translates into a lower bound for the radius ratio:

$$R = \frac{r_c}{r_a} \geq \frac{2}{\sqrt{3}} - 1 \approx 0.1547. \tag{W13A.2}$$

For a cation in the center of a tetrahedron, the anion-to-anion distance is given by $d = a\sqrt{8/3}$. Thus the lower bound for tetrahedral coordination is

$$R \geq \sqrt{\frac{3}{2}} - 1 \approx 0.2247. \tag{W13A.3}$$

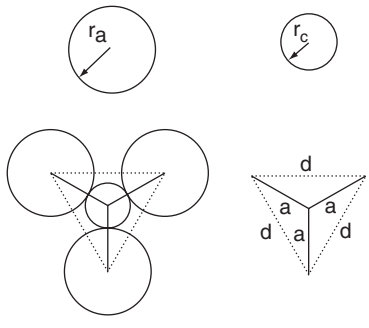

Figure W13A.1. Anions, of radius r_a, surrounding, and in contact with, a cation of radius r_c, forming a planar triangular configuration.

In the sixfold octahedral coordination, $d = a\sqrt{2}$, so it follows that

$$R \geq \sqrt{2} - 1 \approx 0.4142. \tag{W13A.4}$$

In the eightfold cubic coordination, $d = 2a/\sqrt{3}$, so

$$R \geq \sqrt{3} - 1 \approx 0.7321. \tag{W13A.5}$$

REFERENCES

Ternary Phase Diagrams

Hummel, F. A., *Introduction to Phase Equilibria in Ceramics*, Marcel Dekker, New York, 1984.

Silicates

Jaffe, H. W., *Crystal Chemistry and Refractivity*, Dover, Mineola, N.Y., 1996.

Clay

Grimshaw, R. W., *The Chemistry and Physics of Clays and Allied Ceramic Materials*, 4th ed., Wiley-Interscience, New York, 1971.

Cement

Young, Francis, J. ed., Research on cement-based materials, *Mater. Res. Soc. Bull.*, Mar. 1993, p. 33.

PROBLEMS

W13.1 Prove the relations given in Eq. (W13.1) for the ternary phase diagram.

W13.2 Prove the relations given in Eq. (W13.2) for the ternary phase diagram.

W13.3 Referring to Fig. W13.1, prove that $b = c = \frac{1}{2}$ for a material represented by a point midway on the line between components B and C.

W13.4 Referring to Fig. 13.6, show that

$$f_\alpha : f_\beta : f_\gamma = A(\Delta(O\beta\gamma)) : A(\Delta(O\gamma\alpha)) : A(\Delta(O\alpha\beta)),$$

where A is the area of the appropriate triangle.

W13.5 A quaternary phase diagram may be represented as a regular tetrahedron. The four phases are represented by the vertices A, B, C, and D. Show that the composition $A_aB_bC_cD_d$ (with $a + b + c + d = 1$) may be represented by the point O, which is at a perpendicular distance a, b, c, and d from faces BCD, ACD, ABD, and ABC, respectively. Find the length of the edge of the tetrahedron. Can this procedure be generalized to a higher number of components? If so, how?